Engineering Brightness Matched Indium Phosphide Quantum Dots

Reyhaneh Toufanian,

Division of Materials Science and Engineering, Boston University, Boston, MA 02215, USA

Margaret Chern,

Division of Materials Science and Engineering, Boston University, Boston, MA 02215, USA

Victoria H. Kong,

Department of Biomedical Engineering, Boston University, Boston, MA 02215, USA

Allison M. Dennis

Division of Materials Science and Engineering, Boston University, Boston, MA 02215, USA

Department of Biomedical Engineering, Boston University, Boston, MA 02215, USA

Abstract

The size-dependent optoelectronic properties of semiconductor nanocrystals quantum dots (QDs) are hugely beneficial for color tunability but induce an inherent relative PL brightness mismatch in QDs emitting different colors, as larger emitters absorb more incident photons than smaller particles. Here, we examine the effect of core composition, shell composition, and shell thickness on optical properties including high energy absorption, quantum yield (QY), and the relative brightness of InP/ZnS and InP/ZnSe core/shell and InP/ZnSe/ZnS core/shell/shell QDs at different excitation wavelengths. Our analysis reveals that the presence of an intermediate ZnSe shell changes the wavelength of enhanced absorption onset and leads to highly excitation wavelength dependent QYs. Switching from commercial CdSe/ZnS to InP/ZnS reduces the brightness-mismatch between green and red emitters from 33- to 5-fold. Incorporating a 4-monolayer thick optically absorbing ZnSe shell into the QD heterostructure and heating the QDs in a solution of zinc oleate and trioctylphosphine produces InP/ZnSe/ZnS QDs that are ~10-fold brighter than their InP/ZnS counterparts. In contrast to CdSe/CdS/ZnS core/shell/shell QDs, which only photoluminesce at red wavelengths with thicker CdS shells due to their Quasi-Type II bandstructure, Type I InP/ZnSe/ZnS QDs are uniquely suited to creating a rainbow of visible-emitting, brightness matched emitters. By tailoring the thickness of the intermediate ZnSe shell, heavy metal-free, brightness-matched green and red emitters are produced. This study highlights the ability to overcome the inherent brightness mismatch seen in QDs through concerted materials design of heterostructured core/shell InP-based QDs.

Graphical Abstract

Prof. A. M. Dennis, Division of Materials Science and Engineering, Boston University, Boston, MA 02215, USA, aldennis@bu.edu.

Based on their fundamental structure, red-emitting semiconductor quantum dots (QDs) are larger and brighter than green-emitting particles of the same composition. An intermediate ZnSe shell of varying thickness enhances the absorption of InP/ZnSe/ZnS core/shell/shell QDs to produce the first rainbow of brightness-matched, cadmium-free QDs spanning the visible wavelength range.

Brightness Matched Quantum Dots
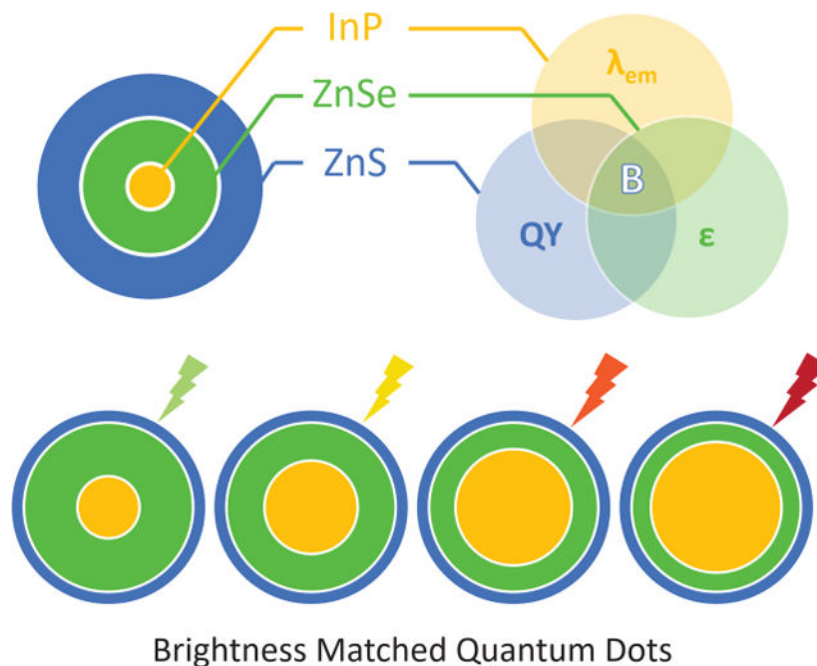
Keywords

semiconductor quantum dots; absorption enhancement; relative brightness; heterostructure; indium phosphide

1. Introduction

Colloidal semiconductor quantum dots (QDs) have garnered extensive research interest as their quantum confinement-based optical properties are compelling for applications ranging from biosensing and imaging to light emitting diodes (LEDs) and displays.[1–5] High absorption cross sections, tunable absorption and emission energies, and narrow emission linewidths, as well as high photo and thermal stability are among advantages of QDs compared to organic dyes.[6,7] While CdSe-based QDs are the most thoroughly studied and optimized, recent developments in the synthesis of near unity quantum yield (QY) InP-based QDs provides an optically competitive alternative,[8–10] with the added benefit of using materials that avoid the cytotoxic effects of CdSe.[11] However, the brightness mismatch of QDs of different emission colors remains a problem, inhibiting multiplexed applications as the intensity from large, red-emitting QDs often overshadows their small blue/green-emitting counterparts.[12,13] On the other hand, utilizing brightness-equalized QDs can enable the simultaneous quantification of multiple mRNA transcripts at the single molecule level in individual cells using fluorescence in situ hybridization (FISH), which is the main technique used for the visualization and quantification of mRNA in cells.[14] Tunable QD brightness

could also be important for instrument-free, low-cost QD sensors with visual readouts designed for diagnostics.[15,16]

The quantum confinement-based spectral tuning of QDs results in an inherent mismatch in the relative brightness (B_{rel}) of the emitters due to differences in their molar extinction coefficient, ε, which scales with the QD volume (*i.e.*, proportional to radius cubed, r^3).[17] At each excitation wavelength (λ_{ex}), B_{rel} is defined as the product of QY (Φ) and the corresponding molar extinction coefficient, ε:[13,18]

$$B_{rel}(\lambda_{ex}) = \varepsilon(\lambda_{ex})\Phi(\lambda_{ex})$$

(1)

Thus, if QDs emitting in a wide spectral range have comparable QY values, differences in extinction coefficients alone can result in significant brightness mismatch. Red-emitting CdSe-based QDs have been shown to emit 48-fold brighter than their green counterparts.[13]

The narrow bandgap of InP (1.35 eV, 919 nm) compared to that of CdSe (1.74 eV, 712 nm), in conjunction with differences in their exciton Bohr radius (10 nm and 5.4 nm for InP and CdSe, respectively), makes it more optically sensitive to changes in the nanocrystal size, providing an intrinsic advantage to solving the brightness mismatch problem. For instance, tuning the lowest energy exciton transition (1S peak) of CdSe core nanocrystals between 495–570 nm, results in a 275% increase in QD volume accompanied by a 3.7-fold change in ε at 400 nm, a standard wavelength for QD excitation (Figure 1A). For InP QDs, however, tuning the 1S peak over a wider spectral range (480–590 nm) results in a smaller change in volume (143%) and 2.5-fold change in ε at 400 nm (Figure 1B, Table S1). This difference in how QD cores of the two materials respond to an increase in size becomes much more pronounced for QD cores with 1S peaks in the 600–700 nm range, as CdSe QDs require larger and larger increases in volume to facilitate optical red-shifting as the particle radius approaches the Bohr radius and the 1S peak approaches the bandgap energy.[15]

As-synthesized InP core nanocrystals, however, are non-emissive (QY < 1%) and highly sensitive to oxidation and humidity, requiring stringent air-free synthesis conditions and necessitating protection with a shell of a second semiconductor material, creating core/shell heterostructures.[19–21] CdSe core nanocrystals, though not as susceptible to oxidation, also require a passivating shell to ensure their long-term stability.[22] ZnS has been a widely used shell material for the passivation of core QDs of various semiconductor materials.[23–29] Given the wide bandgap of ZnS, InP/ZnS and CdSe/ZnS are type-I heterostructures, with exciton confinement in the core.[6] While ZnS deposition results in significant enhancement of photoluminescence (PL) intensity and QY, it only absorbs light at wavelengths shorter than its bulk bandgap of 350 nm, therefore contributing nominally to the QD molar extinction coefficient at 400 nm. Thus, the brightness mismatch between green and red emitters remains a problem for ZnS-shelled heterostructures. In fact, many core/shell CdSe samples have a CdS intermediate shell between the CdSe core and ZnS outer shell. With a bulk bandgap of 498 nm, the CdS layers contribute to absorption at 400 nm, making the difference in absorption cross-section between the green- and red-emitters even more pronounced than is seen for CdSe cores.[30–34] Thicker CdS shells cannot be used to effectively enhance the absorption of smaller, green-emitting CdSe QDs, because the Quasi-

Type II nature of the CdSe/CdS band alignment reduces the bandgap of the core/shell structure relative to the CdSe core, resulting in red-shifting of the emission peak.[44–46]

Similar to CdSe compositions, an intermediate shell between the InP core and ZnS shell can improve the heterostructure properties, largely by bridging the substantial lattice mismatch (7.7%) between InP and ZnS, which can result in strain at the core/shell interface and cause inhomogeneities in shell growth.[35,36] ZnSe has a smaller lattice mismatch with InP (3.4%) and is thus often used as an intermediate shell to create InP/ZnSe/ZnS core/shell/shell heterostructures.[37,38] ZnSe also exhibits a somewhat redder bulk bandgap of 460 nm, meaning that its absorption contributes to the particle molar extinction coefficient at 400 nm, while still maintaining a Type I band alignment in an InP-based core/shell QD.[41]

Here, we report the optical properties of 3 sets of InP-based QD samples (InP/ZnS, InP/ZnSe, and InP/ZnSe/ZnS), which allows a systematic investigation into the effects of shell composition, shell thickness, and excitation energy on the QY, ε, and B_{rel} of the synthesized heterostructures. These studies led to the design of absorption-enhanced visible emitters using InP core nanocrystals of different sizes. We use the variable thickness deposition of intermediate ZnSe shells to tune the absorption cross-section of InP-based core/shell/shell heterostructures to generate brightness-enhanced green emitters and reduce the brightness mismatch of these cadmium-free QDs across the visible wavelength range. A head-to-head comparison of these heterostructures with traditional CdSe/ZnS and InP/ZnS QDs with green to red emission highlights the significance of brightness enhancement and equalization.

2. Results and Discussion

A series of InP-based core/shell and core/shell/shell heterostructures were synthesized to study the effect of shell thickness and composition on the optical properties of QDs. InP core nanocrystals were synthesized according to a previously reported procedure, using a dehalosilylation reaction.[40,41] An empirical fit equation was used to calculate the diameter of the InP core based on the 1S exciton peak position at 533 nm, corresponding to an average diameter of 2.3 nm.[42] As-synthesized InP core nanocrystals are non-emissive and highly susceptible to exposure to oxygen and humidity. To render them emissive, HF etching or passivation using a second semiconductor material are often performed.[43] In this study, 1 to 10 iterations of ZnS or ZnSe deposition using a modified successive ion layer adsorption and reaction (SILAR) method produced core/shell heterostructures with a variety of shell thicknesses. SILAR consists of the addition of cationic and anionic precursors with each precursor addition step followed by a high temperature anneal to ensure the removal of defects from the nanocrystal.[44–46] The amount of precursor added is calculated based on the lattice constant of the shell material and is sufficient for the addition of a single shell monolayer (ML). After 1, 4, 7, and 10 rounds of ZnS or ZnSe shell deposition using zinc oleate and trioctyl phosphine sulfide (TOP:S) or trioctyl phosphine selenide (TOP:Se) as the precursors, respectively, significant volumes were sampled from the InP/ZnS and InP/ZnSe reaction solutions. Although ZnSe shells offer a significantly reduced lattice mismatch, selenium itself is prone to photo-oxidation, making the final heterostructures prone to degradation over time.[47–49] To ensure the long-term stability of these samples, a fraction of

the sample taken from the InP/ZnSe flask was transferred into a clean flask placed under argon for the addition of a second protective ZnS shell using zinc oleate and sulfur dissolved in octadecene to create a core/shell/shell heterostructure. To minimize etching of the InP cores prior to shelling, the first additions of the cationic and anionic precursors were performed at the lower temperature of 150 °C, while precursor addition for all subsequent SILAR iterations was performed at 240 °C.

The 12 synthesized samples (four ZnS shell thicknesses plus four ZnSe shell thicknesses with and without a protective ZnS cap) were imaged using transmission electron microscopy (TEM) (Figure 2). The TEM images demonstrate successful deposition of 3.3 and 4.1 MLs of ZnS and ZnSe shells, respectively, on 2.3 nm diameter InP core nanocrystals after 10 SILAR iterations. The lower efficiency of ZnS shell deposition may be attributed to the large lattice mismatch between the core and shell materials that can give rise to the formation of strain at the core/shell interface as well as to the lower reactivity of TOP:S in comparison to TOP:Se.[39] As can be observed from the TEM images presented here as well as in other studies,[21] the core/shell heterostructures do not have a perfectly spherical morphology. The irregularities in the core/shell heterostructure's morphology are attributed to the formation of an asymmetric oxide layer on the core InP surface, which can form upon exposure of InP to elevated temperatures in the presence of carboxylate precursors. Shell growth on this uneven and amorphous oxide layer may be contributing to the irregular morphology of the QDs.[21,50]

To study the effect of shell deposition on the optical properties of the heterostructures, we collected PL spectra of the twelve samples following excitation at 400 nm. In these type-I heterostructures, the electron and hole are both confined to the narrow bandgap InP core.[41] Thus, the emission color is heavily dictated by the core size, which determines the degree of exciton confinement. The addition of a thin layer of either a ZnS or ZnSe semiconductor shell on the non-emissive InP core was sufficient to produce emissive heterostructures (Figure 3A). As the same InP cores were used for all heterostructures, despite variations in shell thickness and composition, all samples have PL peaks between 565 and 599 nm with the full width at half maximum (FWHM) of the PL peaks decreasing slightly with increased shell thickness (Table 1). After the first iteration of ZnS shell deposition, the PL spectra were dominated by broad trap emission (data not shown), indicating ineffective passivation of the InP core. After one SILAR iteration for InP/ZnSe and four iterations for InP/ZnS, the presence of a substantial red tail indicates incomplete shell deposition and the presence of unpassivated surface trap states.[51] The calculated shell thicknesses based on TEM sizing confirms this, as the average deposited shell thickness after 1 iteration of ZnS and ZnSe shelling is only 0.2 and 0.7 MLs, respectively (Figure 2, Table 1). This red tail in the PL spectra is minimized with further shell deposition, and complete passivation of the core nanocrystal is achieved. ZnS capping of the InP/ZnSe samples resulted in a nominal change in the PL peak position and was accompanied by little to no change in the FWHM of the PL peak.

While the emission profiles of the samples are similar, the same cannot be said for their molar extinction coefficients (ε) (Figure 3B, Figure S1). ε values were estimated by taking absorption measurements of dilutions of cleaned QD solutions and scaling the absorbance spectra to the calculated molar extinction coefficient value of InP at the 1S peak, where InP

is the only component contributing to absorption. QDs exhibit broadband absorption at wavelengths shorter than their bandgap, and their absorption is highly dependent on the number of constituent atoms and bonds.[13] This makes the absorbance of QDs highly dependent on shell thickness, as observed in Figure 3B. For InP/ZnS and InP/ZnSe, an increase in ε is primarily observed at wavelengths shorter than 350 and 460 nm, the bulk bandgaps of ZnS and ZnSe, respectively. The deposition of a protective ZnS cap on the InP/ZnSe nanoparticles through three additional SILAR iterations resulted in further increase of ε. The contribution of ZnSe to absorbance, even at the thinnest shelled samples (InP/1ZnS vs. InP/1ZnSe), resulted in a 40% enhancement of ε at 400 nm. The addition of 4 MLs of ZnSe and an almost 2 ML thick ZnS shell results in a 7-fold enhancement in ε (InP/1ZnS vs. InP/10ZnSe/3ZnS) in otherwise spectrally identical QDs without compromising the emission color or color purity. Given that the brightness of a fluorophore is defined by the product of ε and QY (Equation 1) at a given excitation wavelength (λ_{ex}), an increase in the molar extinction coefficient directly translates into a proportional increase in brightness, if QY is maintained.[34]

In addition to the dependence of molar extinction coefficient on shell composition and thickness, we studied the response of photoluminescence excitation (PLE) spectra to the same variables by monitoring the PL intensity as a function of excitation wavelength (λ_{ex}).[52] In an ideal fluorophore, where excited states emit with equal efficiency, PLE and absorbance spectra should closely resemble one another.[53] Thus, the collected PLE spectra were plotted alongside spectra of the absorption factor, which is one minus transmission (1-T), to elucidate the translation of absorbed light to emitted photons (Figure 4, Figure S2). The absorption factor, also known as absorptance, was calculated from absorbance spectra (A) obtained from the same samples used for the PLE measurements:[54]

$$(1 - T(\lambda_{ex})) = 1 - 10^{-A(\lambda_{ex})} \tag{2}$$

The lowest energy electron transition (1S exciton peak) was chosen as a point of reference and normalized to 1 in each individual PLE and absorption factor spectra. For InP/ZnS samples with 1.1 and 2.0 ML thick ZnS shells, the (1-T) and PLE spectra overlap across a wide spectral range (~350–700 nm). An increase in the absorption factor of InP/ZnS with increasing shell thickness is evident at λ<350 nm, while the same trend is not observed in the PLE spectra. With increasing shell thickness (3.3 ML ZnS), the deviation between (1-T) and PLE becomes pronounced at wavelengths smaller than the bulk bandgap of ZnS.

In InP/ZnSe and InP/ZnSe/ZnS samples, the increase in (1-T) with increasing shell thickness is more pronounced, particularly for λ < 460 nm, the bulk bandgap of ZnSe (Figure 4). For InP/ZnSe, the divergence between (1-T) and PLE at high energy wavelength ranges grows consistently with increasing shell thickness, with the largest deviation seen for the 4.1 ML sample. These observations of gaps between absorption factor and PLE at thicker shells for both InP/ZnS and InP/ZnSe are likely due to the introduction of defects into the crystal structure of the nanoparticle; with increasing shell thicknesses, the formation of defects within the nanoparticle contributing to the non-radiative recombination of electrons and holes becomes more probable.[55] In addition, at higher excitation energies more energy may

be lost to surface trap states which are another site for non-radiative recombination.[56] While the (1-T) and PLE spectra of InP/ZnSe/ZnS closely follow the same trends as InP/ZnSe, the improved passivation offered by the second protective ZnS shell reduces the gap between (1-T) and PLE.

This difference in light absorbed (1-T) and light converted into photons emitted (PLE) is further examined by comparing the excitation wavelength-dependent absolute QYs of the various samples. Measuring the absolute QYs with a six-inch integrating sphere (Quanta-ϕ, Horiba Jobin Yvon) at 350, 400, 450, and 500 nm allows us to distinguish between the efficiency of converting absorbed light into emitted light when it is absorbed exclusively by the InP (500 nm) versus absorption of ZnSe and InP (400 and 450 nm) or absorption by all three compositions (350 nm). Since ZnSe oxidation can negatively affect the measured QYs, InP/ZnSe and InP/ZnSe/ZnS samples cleaned through precipitation and resuspension (PR) were heated with a mixture of zinc oleate and trioctylphosphine.[47–49] This resulted in the notable enhancement of their QY in comparison to those of samples prepared through PR alone (Table S2). Performing the same procedure on InP/ZnS QDs did not notably change QYs (Table S2), further demonstrating the role of selenium oxidation on the samples' optical properties. We observe a clear dependence of QY on λ_{ex}, with QYs at longer excitation wavelengths greater than or equal to the QYs measured for shorter wavelengths (Figure 5). This is consistent with previous reports on λ_{ex} dependence of QYs in the literature, which mainly attribute the lower QYs at higher excitation energies with an increased likelihood of the electrons and holes accessing non-emissive trap states above the QD bandgap.[53,57]

The band structure of type-I QDs minimizes the role of surface-mediated relaxation pathways and of charge transfer to the organic ligands by providing a potential barrier between the electrons and holes photogenerated in the core of the QD and the particle surface, especially at low excitation energies. For InP/ZnS, once the InP core is sufficiently passivated (ZnS shell thickness of at least 2 ML), the QYs are mildly λ_{ex} dependent, but not shell thickness dependent.

Other contributing factors have been linked to λ_{ex} dependence of QYs. For instance, QD aggregation is known to reduce the PL QY since the proximity of QDs in aggregates favors QD-QD energy transfer from small to large QDs, even in samples composed of a narrow size distribution. However, QD-QD energy transfer was avoided by using well-dispersed, dilute samples (absorbance at $\lambda_{ex} < 0.11$), which also minimized inner filter effects and collisional quenching. Scattering caused by the formation of nanoparticles from excess precursors in the reaction solution could also result in the reduction of QY with decreasing λ_{ex}, but no evidence of scattering is observed in the absorbance spectra of these samples (Figure 3).[53,57,58]

For all synthesized samples, the measured QYs at each of the four excitation wavelengths were combined with the corresponding extinction coefficients (Figure 3 and Figure 5) to obtain λ_{ex}-dependent brightness values (Figure 5). Within each shell composition, the contribution of extinction coefficient to B_{rel} at higher excitation energies outweighs the higher QYs at lower excitation energies. Across all samples, the brightest values are obtained at the higher excitation energies, contrary to what is expected based on QY values

alone. This λ_{ex} dependence is especially stark in the case of the thickest shelled InP/ZnSe/ZnS sample (4.1/1.8 ML), where B_{rel} is approximately 9-fold higher at λ_{ex} = 350 nm than at λ_{ex} = 500 nm, in spite of a QY of 20% vs. 47%, respectively. Combining the enhanced absorptivity from ZnSe and the passivating effect of ZnS improves B_{rel} at least 300% at both 350 and 400 nm excitation wavelengths (InP/7ZnS vs. InP/7ZnSe/3ZnS and InP/10ZnS vs. InP/10ZnSe/3ZnS).

These brightness enhancement principles were applied to emitters of different colors to obtain a rainbow of brightness-matched, cadmium-free, visible emitters. In these type-I heterostructures, emission colors are dictated by their core size. Hence, small, medium, large, and extra-large InP core nanocrystals were synthesized with 1S exciton peaks at 447, 497, 565, and 648 nm, respectively. 1, 4, or 7 SILAR iterations for the deposition of ZnSe, followed by 3 iterations of ZnS deposition resulted in core/shell/shell heterostructures with emission colors between 550 and 700 nm, producing green (QD550), yellow (QD570), orange (QD620), and red (QD700) emitters (Table S3, Figure S4). Molar extinction coefficients of these heterostructures were calculated by measuring the absorbance of dilutions of QDs in hexanes, using empirical fit equations for InP core size and molar extinction coefficient to determine the ε_{1S},[6] and using this value to scale the entire absorbance spectrum to ε. By combining ε values with measured QY values at the 400 nm excitation wavelength, the B_{rel} of each sample was calculated (Table S4).

To perform a head-to-head comparison of brightness to more widely used and/or commercially available QD heterostructures, B_{rel} values were calculated for the InP/ZnSe/ZnS core/shell/shell heterostructures as well as CdSe/ZnS and InP/ZnS QDs with comparable emission colors (Figure 6 and Table S4). In data obtained from commercially available CdSe/ZnS QDs (NNCrystal US Corporation), a 33-fold mismatch in B_{rel} was observed between green (QD530) and red (QD665) emitters. This mismatch is a result of significant changes in ε across emitters of different colors, which is an inherent result of spectral tuning using the quantum confinement effect. Across a similar wavelength range (522–666 nm), InP/ZnS QDs exhibited a 5-fold B_{rel} mismatch. (Note: The commercially sourced InP/ZnS emitting at 666 nm had a 18% QY, which was lower than the 30–40% QYs from our lab-made green- and orange-emitting InP/ZnS. Had this sample had a QY of 40%, the brightness mismatch would have been 10-fold, which is still substantially lower than the 33-fold brightness mismatch amongst the commercially sourced CdSe/ZnS samples.) The reduced mismatch in InP/ZnS is a result of the narrow bandgap of InP compared with CdSe, which results in the higher optical sensitivity of InP QDs to changes in size. The brightness disparity in CdSe is compounded by the use of thin CdS bridge shell layers that contribute to the excitonic absorption, and comprise a larger volume when wrapped around larger, redder CdSe cores. With our InP/ZnSe/ZnS QDs, we tune the thickness of the intermediate ZnSe shell contributing to the enhancement of ε at our preferred excitation wavelength (400 nm) to selectively enhance the brightness of the higher energy emitters. By depositing a thick ZnSe shell through 7 SILAR iterations on the smallest InP core with the lowest ε value (QD550) and depositing a thin shell (1 SILAR iteration) on the largest InP core (QD700), we successfully synthesized brightness-equalized green and red emitters. The same ε tuning approach was used to synthesize yellow and orange emitters as well. If QYs are consistent across samples, brightness can be tuned by tuning molar extinction coefficients alone. In

Figure S5, we present the molar extinction coefficients for the different color emitting InP/ZnSe/ZnS QDs with varying ZnSe shell thicknesses. Assuming identical QYs, QDs with similar molar extinction coefficients (denoted by a black box) will inherently be brightness equalized. The ease of estimating the molar extinction coefficient of InP/ZnSe/ZnS heterostructures from the absorbance spectrum facilitates the selection of absorbance-matched samples.

Across the visible wavelength range, we have successfully reduced the 33- and 5-fold brightness mismatch for CdSe/ZnS and InP/ZnS QDs to produce a series of nominally equivalent emitters across the visible wavelength range. This is depicted in Figure 7, where solutions of concentration-matched InP/ZnSe/ZnS QDs demonstrate a reduced mismatch in absorbance at 400 nm as well as PL intensity. While for CdSe/ZnS QDs, the emission from green QDs is buried in the shoulders of their redder emitting counterparts, brightness matching of InP/ZnSe/ZnS QDs results in similar PL intensities for green, yellow, orange, and red InP/ZnSe/ZnS QDs. Thus, the use of an intermediate ZnSe shell is a valuable tool to generate brightness-equalized Type-I heterostructures without compromising emission colors and linewidths. This is in contrast to CdSe/CdS/ZnS QDs, where the Quasi-Type II band structure only results in the generation of red emitting QDs.

3. Conclusions

While the size-dependent tunability of QD photoluminescence is a key feature of this unique optoelectronic material, this fundamental photophysical property also enshrines a brightness mismatch amongst different colors of QDs of the same composition. By examining both CdSe- and InP-based core QDs, we demonstrate that this brightness mismatch can be reduced for visible wavelength emitters by switching core compositions from CdSe to InP. InP exhibits a larger color shift in response to a relatively smaller change in size, resulting in a less substantial change in molar extinction coefficient between green and red emitting QDs. This change in core composition improves the brightness mismatch but cannot be used to create perfectly matched emitters. To fully match brightnesses without compromising quantum yields, we use absorbing shell layers of ZnSe can be used to enhance the molar extinction coefficient of smaller, bluer InP emitters. Our detailed photophysical study of InP heterostructure absorptance vs. PLE demonstrates that the combination of ZnSe and ZnS shelling most effectively mitigates wavelength-dependent differences in light absorption and PLE. Finally, we describe a series of InP/ZnSe/ZnS particles comprising a range of InP core sizes and ZnSe shell thicknesses exhibiting brightness-matched emission. This rainbow of QDs represents the first report of brightness-matched cadmium-free QDs.

Recent advances in InP synthesis enabling the production of QDs with quantum yields and emission bandwidths approaching the high-quality emission achieved with established CdSe chemistry could be combined with this absorption enhancement strategy to produce cadmium-free, visible emitters with exceptional brightness. Utilizing mixtures of QD compositions and concerted engineering of the core/shell heterostructure, the photoluminescence brightness mismatch that is otherwise inherent for semiconductor QDs can be overcome.

4. Materials and Methods

Materials:

Oleylamine (OAm, technical grade, 70%), 1-octadecene (ODE, 90%), sulfur (S, 99.999%), and hexanes (99%) were purchased from Fisher Scientific. Tris(trimethylsilyl) phosphine ((TMS)$_3$P, 98%) was purchased from Strem Chemical, Inc. Chloroform was purchased from J.T.Baker. Indium (III) acetate (In(Ac)$_3$, 99.99%), oleic acid (OA, 90%), n-trioctylphosphine (TOP, 97%), selenium pellets (Se, 99.99%), zinc acetate (Zn(Ac)$_2$, 99.0%), indium (III) acetylacetonate (In(Acac)$_3$, 99.99%), trioctylphosphine oxide (TOPO, 99%), myristic acid (HMy, 99%), ethanol (99.8%), dioctylamine (97%), and InP/ZnS QDs (λ_{em}=670 nm) in toluene were purchased from Sigma-Aldrich. ODE was heated to 120 °C under vacuum for several hours with multiple argon backfill and evacuation cycles to ensure complete removal of air and water and stored in an argon glovebox prior to use. CdSe/ZnS QDs were purchased from NNCrystal US Corporation. All other chemicals were used directly without further purification. Quartz cuvettes were purchased from Starna Cells Inc. All air-sensitive materials were stored and handled in an argon glovebox.

Precursors:

The metal and chalcogenide precursors were prepared with minor modifications to previously reported protocols.[41] A 0.2 M stock solution of indium oleate (In:OA=1:3.3) was prepared by mixing indium (III) acetate (3.2 mmol, 0.93 g) and oleic acid (10.61 mmol, 3.35 mL) and heating the reaction flask to 120 °C under vacuum for two hours with multiple argon backfill and evacuation cycles to ensure the complete removal of acetic acid. After a clear and colorless solution was obtained, degassed ODE (12.58 mL) was added to the solution. Once the temperature of the solution reached 120 °C, it was cooled to 90 °C and vacuumed for another hour. The precursor was stored under argon and heated to 60 °C when in use.

A 0.2 M stock solution of zinc oleate (Zn:OA=1:4) was prepared by mixing zinc acetate (20 mmol, 4.39 g) with oleic acid (88.88 mmol, 28.05 mL) and degassing under vacuum at room temperature until no vigorous bubbling was observed. The temperature was raised to 120 °C and maintained for 2 hours, until the solution was clear, and no bubbling was observed. Multiple argon backfills and evacuation cycles were performed to ensure complete removal of acetic acid. At this point, degassed ODE (71.95 mL) was added to the solution and vacuumed for another hour. The precursor solution is solid at room temperature and was stored under argon and heated to at 95 °C when in use. A 0.2 M stock solution of zinc oleate (Zn:OA=1:4) was prepared in the same manner for the post synthetic treatment of the samples, where the Zn(OA)$_2$ mixture was diluted using TOP instead of ODE. This precursor solution was stored at room temperature under argon flow.

0.2 M stock solutions of sulfur in both TOP and ODE were used as sulfur precursors. For the preparation of a 0.2 M stock solution of sulfur in ODE, elemental sulfur (3.11 mmol, 0.1 g) and ODE (15.59 mL) were mixed and heated to 80 °C under vacuum for 1 hour. The flask was backfilled with argon and heated at 80 °C overnight to ensure complete dissolution of sulfur in ODE and stored at the same temperature for future use. 0.2 M stock solutions of

sulfur in TOP and selenium in TOP were prepared in glass vials on a hot plate in an argon filled glovebox by heating at 80 °C with stirring overnight.

Synthesis of CdSe Core Nanocrystals (First Exciton Absorption Peaks Between 495–570 nm):

CdSe core nanocrystals were synthesized based on a previously reported method.[44] TOPO (1 g), ODE (8 mL), and Cd(OA)$_2$ (0.38 mmol) were loaded into a 100 mL round bottom flask and vacuumed at room temperature for 30 minutes. The temperature was then raised to 80 °C and heated for an additional 30 minutes. The flask was backfilled with argon and the temperature was raised to 300 °C. TOP:Se (4 mmol), OAm (3 mL), and ODE (1 mL) were mixed in an argon glovebox and loaded into a syringe. This solution was swiftly injected into the flask. Samples were taken at different time points to generate a size series of CdSe core nanocrystals with first exciton peaks between 495–570 nm. The reaction was stopped by cooling the flask to room temperature.

Synthesis of InP Core Nanocrystals (First Exciton Absorption Peaks Between 480–590 nm):

InP core nanocrystals were synthesized by modifying a previously reported method.[8] In(Acac)$_3$ (0.174 g), HMy (0.193 g), and ODE (7 mL) were loaded into a 100 mL round bottom flask in an argon glovebox. The flask was taken out of the glovebox and connected to a Schlenk line. The solution was stirred at room temperature for 10 minutes and heated at 160 °C for 20 minutes. A solution containing medium sized InP cores with a first exciton peak at 497 nm (200 nmoles) was loaded into a syringe and swiftly added to the flask. After 20 minutes, 0.1 M (TMS)$_3$P (7 mL) was slowly added to the reaction flask using a stepper motor syringe pump at a rate of 1 mL/hour. Samples were taken at different time points to make a size series of InP core nanocrystals with first exciton peaks between 480–590 nm. The reaction was stopped by cooling it to room temperature.

Synthesis of InP Core Nanocrystals (First Exciton Absorption Peaks Between 441–648 nm):

InP core nanocrystals of four different sizes –small, medium, large, and extra-large (S, M, L, and XL, respectively) were synthesized based on a previously reported hot injection method. [41] For the synthesis of the small, medium, and large cores, 0.2 M In(OA)$_3$ (2 mL), OAm (1.5 mL), and ODE (4 mL) were loaded into a 100 mL round bottom flask and heated under vacuum to 120 °C with multiple argon backfills, while syringes of 0.1 M and 1 M (TMS)$_3$P in ODE were prepared in the glovebox. An initial amount of 1 M (TMS)$_3$P (0.2 mL) was rapidly injected into each flask of indium oleate at 191 °C with the thermocouples set to 178 °C for the growth phase of the reaction. Starting at 45 seconds of the first injection, 0.1 M (TMS)$_3$P (2 mL) was added to the flask via dropwise injection. Small cores were reliably produced by quenching this reaction after 3.5 minutes by removing the heating mantle and swiftly adding degassed, room temperature ODE (12 mL). To generate medium and large cores, more indium and phosphorus was repeatedly added to the InP cores to provide precursors for growth in separate aliquots. For medium cores, 0.2 M In(OA)$_3$ (4 mL) and 0.1 M (TMS)$_3$P (4 mL) were added over the span of 12 minutes. For large cores, 0.2 M In(OA)$_3$ (12 mL) and 0.1 M (TMS)$_3$P (12 mL) were added over 23.5 minutes. After 13.5 and 32

minutes of total reaction time for medium and large cores, respectively, the reaction was quenched by removing the heating mantle and adding degassed, room temperature ODE (12 and 24 mL for medium and large cores, respectively).

For the synthesis of extra-large InP cores, 0.2 M In(OA)$_3$ (2 mL), dioctylamine (0.5 mL), and ODE (4 mL) were loaded into a 100 mL round bottom flask and heated under vacuum to 120 °C with multiple argon backfills. 1 M (TMS)$_3$P (0.2 mL) was rapidly injected into the flask of indium oleate at 191 °C with the thermocouples set to 178 °C for the growth phase of the reaction. Starting at 45 seconds of the first injection, 0.1 M (TMS)$_3$P (2 mL) was added to the flask via dropwise injection. The flask was heated at 178 °C for 14 hours and the reaction was stopped by cooling it down to room temperature.

These reactions yielded InP core nanocrystals with 1S exciton peaks at 441 (S), 497 (M), 533 and 565 (L), and 648 (XL) nm. InP cores with a 533 nm 1S peak were used to generate InP/ZnS, InP/ZnSe, and InP/ZnSe/ZnS samples to study the effect of shell composition and thickness on ε, QY, and B$_{rel}$. The remaining four core sizes were used for the synthesis of brightness equalized InP/ZnSe/ZnS core/shell/shell heterostructures. To remove any precipitates from the reaction products, the solutions containing InP core nanocrystals were transferred into a clean centrifuge tube and centrifuged for 15 minutes at ~2600 rcf in an argon glovebox. The supernatant was saved for future use. The samples were stored in an argon glovebox at 4 °C.

Synthesis of Core/Shell Nanocrystals:

Two distinct shell compositions comprising ZnSe and ZnS were deposited on InP core nanocrystals using a modified successive ion layer adsorption and reaction (SILAR) technique, adapted for colloidal synthesis.[46] In this approach, aliquots of cationic and anionic precursors were added to the core solution between long anneals at growth temperatures (150–240 °C). The required amounts of anion and cation precursors were calculated based on the number of surface atoms needed to add a monolayer to a certain size of a core/shell nanocrystal. For each reaction, OAm (1 mL) and enough ODE to make up a total reaction volume of 10 mL were mixed in a 100 mL round bottom flask on a Schlenk line. The flask was vacuumed at room temperature for 30 minutes before the solution temperature was raised to 120 °C under vacuum for 30 minutes with multiple vacuum/argon cycles. The flask was backfilled with argon and the temperature was raised to 150 °C for the deposition of the first shell monolayer. To protect the InP cores from Ostwald ripening caused by prolonged exposure to heat, the cores were injected at 150 °C. Shell deposition was started immediately after the temperature stabilized.

For all shell compositions, the cation and anion precursors for the first shell deposition was injected at 150 °C; the first anion injection proceeded 10 min after the cation injection. Immediately after the anion injection, the temperature was raised to 240 °C and the solution was annealed for 1 hour. All subsequent shell precursors were injected dropwise at 240 °C, followed by annealing for 2.5 hours after the cation injection, and 1 hour after the anion injection. To monitor the progress of the reaction, aliquots of the reaction solutions were taken at regular intervals. Once the desired shell thickness was reached, the InP/ZnSe samples were capped with a second ZnS protective shell with 3 iterations of SILAR using

0.2 M $Zn(OA)_2$ and 0.2 M S8/ODE or 0.2 M TOP:S at 240 °C. The reactions were terminated by cooling the solution to room temperature.

QD Sample Preparation:

Solutions of raw QD solutions were diluted in hexanes or chloroform at a 1:5 ratio and centrifuged at ~2,500 rcf for 3 minutes. The supernatant was transferred to a clean microcentrifuge tube and a 1:5 ratio of ethanol was added to the tube and centrifuged at ~22,000 rcf for 7 minutes. The clear supernatant was decanted and the QD pellet was resuspended in hexanes or chloroform.

QD samples used for QY measurements were incubated at 85 °C for 2 hours in a water bath with a 1:1 v/v ratio of QD:TOP prior to centrifugation. After the sample was centrifuged at ~22,000 rcf for 4 minutes, the supernatant was transferred into a new tube, and a 1:5 ratio of ethanol was added to the tube. The solution was then centrifuged at ~22,000 rcf for 7 minutes. The clear supernatant was discarded and the QD pellet was suspended to its original volume in 0.2 M $Zn(OA)_2$ in TOP and incubated at 85 °C for 2 hours.

Determination of Molar Extinction Coefficients and QD Concentrations:

In order to determine the concentration of QD solutions, knowledge of their molar extinction coefficient at different excitation wavelengths, $\varepsilon(\lambda_{ex})$, was required. To this end, absorbance measurements were taken of purified QD solutions. The location of the 1S peak and absorbance intensity at that wavelength was determined. Using published empirical fit equations for both CdSe and InP,[6] the molar extinction coefficient of the QD at the 1S peak, where the InP or CdSe core is the only component of the QD contributing to absorbance, was determined. For the preparation of Figure 3, which depicts QD molar extinction coefficients as a function of wavelength, the absorbance spectra obtained from each QD sample was scaled to its corresponding molar extinction coefficient at the 1S peak. The Beer-Lambert Law was used to determine the concentration of QDs in solution using the sample-specific, calculated molar extinction coefficient and an absorbance measurement of the solution. Concentration-matched solutions of QD heterostructures were prepared by performing further dilutions of QDs in controlled amounts of hexane.

QD Characterization:

Absorption measurements of samples purified by precipitation and resuspension were performed using a NanoDrop™ 2000c (Thermo Scientific) spectrophotometer and converted to absorptance, or absorption factor, using Equation 2.

Photoluminescence and photoluminescence excitation spectroscopy were performed using a Horiba Jobin Yvon NanoLog spectrofluorometer outfitted with a 450 W Xenon arc lamp, double excitation and emission monochromators, and silicon CCD detector. QD samples were precipitated with ethanol and suspended in chloroform in quartz cuvettes. The collected spectra were corrected for lamp power and detector sensitivity using the supplied correction files. Absolute quantum yield values were obtained using the spectrofluorometer described above with a Quanta-phi six-inch integrating sphere. Cuvettes were loaded with hexanes in order to generate a blank reference following excitation at 350, 400, 450, and 500

nm. QD samples were diluted directly into the blanked cuvettes and measured under identical conditions. All measurements were performed using 5 averaged scans. The absorbance of each sample at the excitation wavelength was below 0.11. The absolute quantum yield (i.e., the number of photons emitted divided by the photons absorbed) was determined using the Horiba software.

Transmission electron microscopy (TEM) images were acquired using the JEOL ARM 200F STEM and the JEOL 2100 LaB6 high-resolution microscopes operating at 200 kV. Each sample was precipitated using ethanol and resuspended in hexanes and drop-cast on a copper TEM grid, which was washed successively by hexane, ethanol, and DI water. The grid was then gently heated to evaporate any residual water. TEM images were sized manually using ImageJ by determining the area enclosed within an outline drawn around the particle and backcalculating the diameter assuming a spherical nanocrystal. TEM images in Figure 1 have been size-matched for presentation, and the reported average diameters, standard deviations, and percent errors are based on the sizing of 104–153 QDs.

Images of samples with concentration-matched solutions within each composition (11.6 nM for CdSe/ZnS, 46.5 nM for InP/ZnS and InP/ZnSe/ZnS samples) were taken using a Canon EOS R mirrorless digital camera. To depict NIR emission from QD700, the image was also taken of the same samples using a Canon PowerShot A630 with the infrared-cut filter removed. All images were taken with the addition of a 450 nm long pass filter to eliminate UV light from the excitation source.

Supplementary Material

Refer to Web version on PubMed Central for supplementary material.

Acknowledgements

References

(1). Chern M; Kays JC; Bhuckory S; Dennis AM Sensing with Photoluminescent Semiconductor Quantum Dots. Methods Appl. Fluoresc 2019, 7 (1), 012005. 10.1088/2050-6120/aaf6f8. [PubMed: 30530939]

(2). Bhuckory S; Kays JC; Dennis AM In Vivo Biosensing Using Resonance Energy Transfer. Biosensors 2019, 9 (2), 76. 10.3390/bios9020076.

(3). Li J; Zhu J-J Quantum Dots for Fluorescent Biosensing and Bio-Imaging Applications. Analyst 2013, 138 (9), 2506. 10.1039/c3an36705c. [PubMed: 23518695]

(4). Wu Z; Liu P; Zhang W; Wang K; Sun XW Development of InP Quantum Dot-Based Light-Emitting Diodes. ACS Energy Lett. 2020, 5 (4), 1095–1106. 10.1021/acsenergylett.9b02824.

(5). Jang E; Kim Y; Won Y-H; Jang H; Choi S-M Environmentally Friendly InP-Based Quantum Dots for Efficient Wide Color Gamut Displays. ACS Energy Lett. 2020, 5 (4), 1316–1327. 10.1021/acsenergylett.9b02851.

(6). Reiss P; Protière M; Li L Core/Shell Semiconductor Nanocrystals. Small 2009, 5 (2), 154–168. 10.1002/smll.200800841. [PubMed: 19153991]

(7). Resch-Genger U; Grabolle M; Cavaliere-Jaricot S; Nitschke R; Nann T Quantum Dots versus Organic Dyes as Fluorescent Labels. Nat. Methods 2008, 5 (9), 763–775. 10.1038/nmeth.1248. [PubMed: 18756197]

(8). Li Y; Hou X; Dai X; Yao Z; Lv L; Jin Y; Peng X Stoichiometry-Controlled InP-Based Quantum Dots: Synthesis, Photoluminescence, and Electroluminescence. J. Am. Chem. Soc 2019, 141 (16), 6448–6452. 10.1021/jacs.8b12908. [PubMed: 30964282]

(9). Xu Z; Li Y; Li J; Pu C; Zhou J; Lv L; Peng X Formation of Size-Tunable and Nearly Monodisperse InP Nanocrystals: Chemical Reactions and Controlled Synthesis. Chem. Mater 2019, 31 (14), 5331–5341. 10.1021/acs.chemmater.9b02292.

(10). Won YH; Cho O; Kim T; Chung DY; Kim T; Chung H; Jang H; Lee J; Kim D; Jang E Highly Efficient and Stable InP/ZnSe/ZnS Quantum Dot Light-Emitting Diodes. Nature 2019, 575 (7784), 634–638. 10.1038/s41586-019-1771-5. [PubMed: 31776489]

(11). Atha DH; Nagy A; Steinbrück A; Dennis AM; Hollingsworth JA; Dua V; Iyer R; Nelson BC Quantifying Engineered Nanomaterial Toxicity: Comparison of Common Cytotoxicity and Gene Expression Measurements. J. Nanobiotechnology 2017, 15 (1), 1–9. 10.1186/s12951-017-0312-3. [PubMed: 28049488]

(12). Kairdolf BA; Smith AM; Stokes TH; Wang MD; Young AN; Nie S Semiconductor Quantum Dots for Bioimaging and Biodiagnostic Applications. Annu. Rev. Anal. Chem 2013, 6 (1), 143–162. 10.1146/annurev-anchem-060908-155136.

(13). Lim SJ; Zahid MU; Le P; Ma L; Entenberg D; Harney AS; Condeelis J; Smith AM Brightness-Equalized Quantum Dots. Nat. Commun 2015, 6 (1), 8210. 10.1038/ncomms9210. [PubMed: 26437175]

(14). Liu Y; Le P; Lim SJ; Ma L; Sarkar S; Han Z; Murphy SJ; Kosari F; Vasmatzis G; Cheville JC; Smith AM Enhanced MRNA FISH with Compact Quantum Dots. Nat. Commun 2018, 9 (1). 10.1038/s41467-018-06740-x.

(15). Chern M; Toufanian R; Dennis AM Quantum Dot to Quantum Dot Förster Resonance Energy Transfer: Engineering Materials for Visual Color Change Sensing. Analyst 2020, 145 (17), 5754–5767. 10.1039/d0an00746c. [PubMed: 32715305]

(16). Chern M; Garden PM; Baer RC; Galagan JE; Dennis AM Transcription Factor Based Small-Molecule Sensing with a Rapid Cell Phone Enabled Fluorescent Bead Assay. Angew. Chemie - Int. Ed 2020, 2–8. 10.1002/anie.202007575.

(17). Karel apek R; Moreels I; Lambert K; De Muynck D; Zhao Q; Van Tomme A; Vanhaecke F; Hens Z Optical Properties of Zincblende Cadmium Selenide Quantum Dots. J. Phys. Chem. C 2010, 114 (14), 6371–6376. 10.1021/jp1001989.

(18). Würth C; Pauli J; Lochmann C; Spieles M; Resch-Genger U Integrating Sphere Setup for the Traceable Measurement of Absolute Photoluminescence Quantum Yields in the Near Infrared. Anal. Chem 2012, 84 (3), 1345–1352. 10.1021/ac2021954. [PubMed: 22242570]

(19). Tamang S; Lincheneau C; Hermans Y; Jeong S; Reiss P Chemistry of InP Nanocrystal Syntheses. Chem. Mater 2016, 28 (8), 2491–2506. 10.1021/acs.chemmater.5b05044.

(20). Hahm D; Chang JH; Jeong BG; Park P; Kim J; Lee S; Choi J; Kim WD; Rhee S; Lim J; Lee DC; Lee C; Char K; Bae WK Design Principle for Bright, Robust, and Color-Pure InP/ZnSe x S 1-x /ZnS Heterostructures. Chem. Mater 2019, 31 (9), 3476–3484. 10.1021/acs.chemmater.9b00740.

(21). Reid KR; McBride JR; Freymeyer NJ; Thal LB; Rosenthal SJ Chemical Structure, Ensemble and Single-Particle Spectroscopy of Thick-Shell InP–ZnSe Quantum Dots. Nano Lett. 2018, acs.nanolett.7b03703. 10.1021/acs.nanolett.7b03703.

(22). Wang K; He W; Wu L; Xu G; Ji S; Ye C On the Stability of CdSe Quantum Dot-Sensitized Solar Cells. RSC Adv. 2014, 4 (30), 15702. 10.1039/c4ra01846j.

(23). Xu S; Ziegler J; Nann T Rapid Synthesis of Highly Luminescent InP and InP/ZnS Nanocrystals. J. Mater. Chem 2008, 18 (23), 2653. 10.1039/b803263g.

(24). Tessier MD; Dupont D; De Nolf K; De Roo J; Hens Z Economic and Size-Tunable Synthesis of InP/ZnE (E = S, Se) Colloidal Quantum Dots. Chem. Mater 2015, 27 (13), 4893–4898. 10.1021/acs.chemmater.5b02138.

(25). Chuang P-H; Lin CC; Liu R-S Emission-Tunable CuInS 2 /ZnS Quantum Dots: Structure, Optical Properties, and Application in White Light-Emitting Diodes with High Color Rendering Index. ACS Appl. Mater. Interfaces 2014, 6 (17), 15379–15387. 10.1021/am503889z. [PubMed: 25111960]

(26). Dabbousi BO; Rodriguez-Viejo J; Mikulec FV; Heine JR; Mattoussi H; Ober R; Jensen KF; Bawendi MG (CdSe)ZnS Core–Shell Quantum Dots: Synthesis and Characterization of a Size Series of Highly Luminescent Nanocrystallites. J. Phys. Chem. B 1997, 101 (46), 9463–9475. 10.1021/jp971091y.

(27). Boercker JE; Woodall DL; Cunningham PD; Placencia D; Ellis CT; Stewart MH; Brintlinger TH; Stroud RM; Tischler JG Synthesis and Characterization of PbS/ZnS Core/Shell Nanocrystals. Chem. Mater 2018, 30 (12), 4112–4123. 10.1021/acs.chemmater.8b01421.

(28). Dong B; Cao L; Su G; Liu W Facile Synthesis of Highly Luminescent UV-Blue Emitting ZnSe/ZnS Core/Shell Quantum Dots by a Two-Step Method. Chem. Commun 2010, 46 (39), 7331. 10.1039/c0cc02042g.

(29). Ji B; Koley S; Slobodkin I; Remennik S; Banin U ZnSe/ZnS Core/Shell Quantum Dots with Superior Optical Properties through Thermodynamic Shell Growth. Nano Lett. 2020, 20 (4), 2387–2395. 10.1021/acs.nanolett.9b05020. [PubMed: 32134676]

(30). Mohan S; Oluwafemi OS; Songca SP; Osibote OA; George SC; Kalarikkal N; Thomas S Facile Synthesis of Transparent and Fluorescent Epoxy-CdSe-CdS-ZnS Core-Multi Shell Polymer Nanocomposites. New J. Chem 2014, 38 (1), 155–162. 10.1039/c3nj00659j.

(31). Lim SJ; Chon B; Joo T; Shin SK Synthesis and Characterization of Zinc-Blende CdSe-Based Core/Shell Nanocrystals and Their Luminescence in Water. J. Phys. Chem. C 2008, 112 (6), 1744–1747. 10.1021/jp710648g.

(32). Wang X; Li W; Sun K Stable Efficient CdSe/CdS/ZnS Core/Multi-Shell Nanophosphors Fabricated through a Phosphine-Free Route for White Light-Emitting-Diodes with High Color Rendering Properties. J. Mater. Chem 2011, 21 (24), 8558–8565. 10.1039/c1jm00061f.

(33). Naughton MS; Kumar V; Bonita Y; Deshpande K; Kenis PJA High Temperature Continuous Flow Synthesis of CdSe/CdS/ZnS, CdS/ZnS, and CdSeS/ZnS Nanocrystals. Nanoscale 2015, 7 (38), 15895–15903. 10.1039/c5nr04510j. [PubMed: 26361342]

(34). Chern M; Nguyen TT; Mahler AH; Dennis AM Shell Thickness Effects on Quantum Dot Brightness and Energy Transfer. Nanoscale 2017, 9 (42), 16446–16458. 10.1039/C7NR04296E. [PubMed: 29063928]

(35). Rafipoor M; Dupont D; Tornatzky H; Tessier MD; Maultzsch J; Hens Z; Lange H Strain Engineering in InP/(Zn,Cd)Se Core/Shell Quantum Dots. Chem. Mater 2018, 30 (13), 4393–4400. 10.1021/acs.chemmater.8b01789.

(36). Jo J-H; Jo D-Y; Lee S-H; Yoon S-Y; Lim H-B; Lee B-J; Do YR; Yang H InP-Based Quantum Dots Having an InP Core, Composition-Gradient ZnSeS Inner Shell, and ZnS Outer Shell with Sharp, Bright Emissivity, and Blue Absorptivity for Display Devices. ACS Appl. Nano Mater 2020, 3 (2), 1972–1980. 10.1021/acsanm.0c00008.

(37). Kim Y; Ham S; Jang H; Min JH; Chung H; Lee J; Kim D; Jang E Bright and Uniform Green Light Emitting InP/ZnSe/ZnS Quantum Dots for Wide Color Gamut Displays. ACS Appl. Nano Mater 2019, 2 (3), 1496–1504. 10.1021/acsanm.8b02063.

(38). Hahm D; Chang JH; Jeong BG; Park P; Kim J; Lee S; Choi J; Kim WD; Rhee S; Lim J; Lee DC; Lee C; Char K; Bae WK Design Principle for Bright, Robust, and Color-Pure InP/ZnSe x S 1-x /ZnS Heterostructures-SI. Chem. Mater 2019, 31 (9), 3476–3484. 10.1021/acs.chemmater.9b00740.

(39). Lim J; Bae WK; Lee D; Nam MK; Jung J; Lee C; Char K; Lee S InP@ZnSeS, Core@composition Gradient Shell Quantum Dots with Enhanced Stability. Chem. Mater 2011, 23 (20), 4459–4463. 10.1021/cm201550w.

(40). Dennis AM; Mangum BD; Piryatinski A; Park Y; Hannah DC; Casson JL; Williams DJ; Schaller RD; Htoon H; Hollingsworth JA Suppressed Blinking and Auger Recombination in Near-Infrared Type-II InP/CdS Nanocrystal Quantum Dots. Nano Lett. 2012, 12 (11), 5545–5551. 10.1021/nl302453x. [PubMed: 23030497]

(41). Toufanian R; Piryatinski A; Mahler AH; Iyer R; Hollingsworth JA; Dennis AM Bandgap Engineering of Indium Phosphide-Based Core/Shell Heterostructures Through Shell Composition and Thickness. Front. Chem 2018, 6 (NOV). 10.3389/fchem.2018.00567.

(42). Xie R; Li Z; Peng X Nucleation Kinetics vs Chemical Kinetics in the Initial Formation of Semiconductor Nanocrystals. J. Am. Chem. Soc 2009, 131 (42), 15457–15466. 10.1021/ja9063102. [PubMed: 19775131]

(43). Janke EM; Williams NE; She C; Zherebetskyy D; Hudson MH; Wang L; Gosztola DJ; Schaller RD; Lee B; Sun C; Engel GS; Talapin DV Origin of Broad Emission Spectra in InP Quantum Dots: Contributions from Structural and Electronic Disorder. J. Am. Chem. Soc 2018, 140 (46), 15791–15803. 10.1021/jacs.8b08753. [PubMed: 30285448]

(44). Ghosh Y; Mangum BD; Casson JL; Williams DJ; Htoon H; Hollingsworth JA New Insights into the Complexities of Shell Growth and the Strong Influence of Particle Volume in Nonblinking "Giant" Core/Shell Nanocrystal Quantum Dots. J. Am. Chem. Soc 2012, 134 (23), 9634–9643. 10.1021/ja212032q. [PubMed: 22578279]

(45). Chen Y; Vela J; Htoon H; Casson JL; Werder DJ; Bussian DA; Klimov VI; Hollingsworth JA "Giant" Multishell CdSe Nanocrystal Quantum Dots with Suppressed Blinking. J. Am. Chem. Soc 2008, 130 (15), 5026–5027. 10.1021/ja711379k. [PubMed: 18355011]

(46). Li JJ; Wang YA; Guo W; Keay JC; Mishima TD; Johnson MB; Peng X Large-Scale Synthesis of Nearly Monodisperse CdSe/CdS Core/Shell Nanocrystals Using Air-Stable Reagents via Successive Ion Layer Adsorption and Reaction. 2003. 10.1021/ja0363563.

(47). Jana S; Srivastava BB; Acharya S; Santra PK; Jana NR; Sarma DD; Pradhan N Prevention of Photooxidation in Blue–Green Emitting Cu Doped ZnSe Nanocrystals. Chem. Commun 2010, 46 (16), 2853. 10.1039/b925980e.

(48). Cooper JK; Gul S; Lindley SA; Yano J; Zhang JZ Tunable Photoluminescent Core/Shell Cu + -Doped ZnSe/ZnS Quantum Dots Codoped with Al 3+, Ga 3+, or In 3+. ACS Appl. Mater. Interfaces 2015, 7 (18), 10055–10066. 10.1021/acsami.5b02860. [PubMed: 25893312]

(49). Jia J; Xue P; Hu X; Wang Y; Liu E; Fan J Electron-Transfer Cascade from CdSe@ZnSe Core-Shell Quantum Dot Accelerates Photoelectrochemical H2 Evolution on TiO2 Nanotube Arrays. J. Catal 2019, 375, 81–94. 10.1016/j.jcat.2019.05.028.

(50). Cros-Gagneux A; Delpech F; Nayral C; Cornejo A; Coppel Y; Chaudret B Surface Chemistry of InP Quantum Dots: A Comprehensive Study. J. Am. Chem. Soc 2010, 132 (51), 18147–18157. 10.1021/ja104673y. [PubMed: 21126088]

(51). Thomas A; Sandeep K; Somasundaran SM; Thomas KG How Trap States Affect Charge Carrier Dynamics of CdSe and InP Quantum Dots: Visualization through Complexation with Viologen. ACS Energy Lett. 2018, 3 (10), 2368–2375. 10.1021/acsenergylett.8b01532.

(52). Crouch CH; Mohr R; Emmons T; Wang S; Drndic M Excitation Energy Dependence of Fluorescence Intermittency in CdSe/ZnS Core–Shell Nanocrystals. J. Phys. Chem. C 2009, 113 (28), 12059–12066. 10.1021/jp8104216.

(53). Hoy J; Morrison PJ; Steinberg LK; Buhro WE; Loomis RA Excitation Energy Dependence of the Photoluminescence Quantum Yields of Core and Core/Shell Quantum Dots. J. Phys. Chem. Lett 2013, 4 (12), 2053–2060. 10.1021/jz4004735. [PubMed: 26283252]

(54). Resch-Genger U; DeRose PC Characterization of Photoluminescence Measuring Systems (IUPAC Technical Report). Pure Appl. Chem 2012, 84 (8), 1815–1835. 10.1351/PAC-REP-10-07-07.

(55). Mulder JT; Kirkwood N; De Trizio L; Li C; Bals S; Manna L; Houtepen AJ Developing Lattice Matched ZnMgSe Shells on InZnP Quantum Dots for Phosphor Applications. ACS Appl. Nano Mater 2020, 3 (4), 3859–3867. 10.1021/acsanm.0c00583. [PubMed: 32363330]

(56). Roy D; Das A; De CK; Mandal S; Ranjan Bangal P; Mandal PK Why Does the Photoluminescence Efficiency Depend on Excitation Energy in Case of a Quantum Dot? A Case Study of CdSe-Based Core/Alloy Shell/Shell Quantum Dots Employing Ultrafast Pump– Probe Spectroscopy and Single Particle Spectroscopy. 2019. 10.1021/acs.jpcc.9b00422.

(57). Martynenko IV; Baimuratov AS; Osipova VA; Kuznetsova VA; Purcell-Milton F; Rukhlenko ID; Fedorov AV; Gun'ko YK; Resch-Genger U; Baranov AV Excitation Energy Dependence of the

Photoluminescence Quantum Yield of Core/Shell CdSe/CdS Quantum Dots and Correlation with Circular Dichroism. Chem. Mater 2018, 30 (2), 465–471. 10.1021/acs.chemmater.7b04478.

(58). Leatherdale CA; Woo W-K; Mikulec FV; Bawendi MG On the Absorption Cross Section of CdSe Nanocrystal Quantum Dots. J. Phys. Chem. B 2002, 106 (31), 7619–7622. 10.1021/jp025698c.

(59). Extinction coefficients of Qdot nanocrystal streptavidin conjugates at ultraviolet and visible wavelengths—Table 6.10 | Thermo Fisher Scientific - US https://www.thermofisher.com/us/en/home/references/molecular-probes-the-handbook/tables/extinction-coefficients-of-qdot-streptavidin-conjugates-at-common-wavelengths.html (accessed Jun 2, 2020).

(60). InP/ZnS quantum dots stabilized with oleylamine ligands, fluorescence λem 650 nm, 5 mg/mL in toluene | Cadmium free quantum dots | Sigma-Aldrich https://www.sigmaaldrich.com/catalog/product/aldrich/776785?lang=en&region=US (accessed Jun 2, 2020).
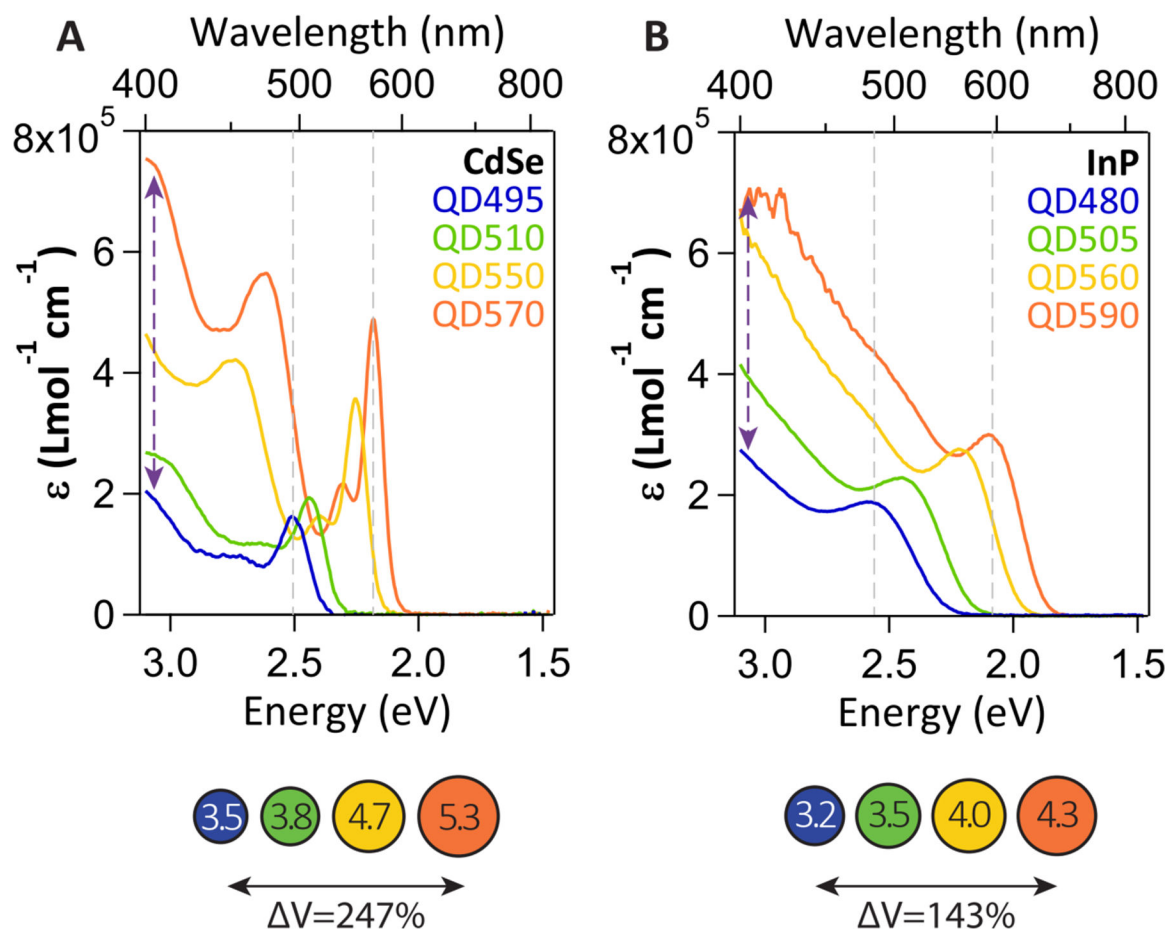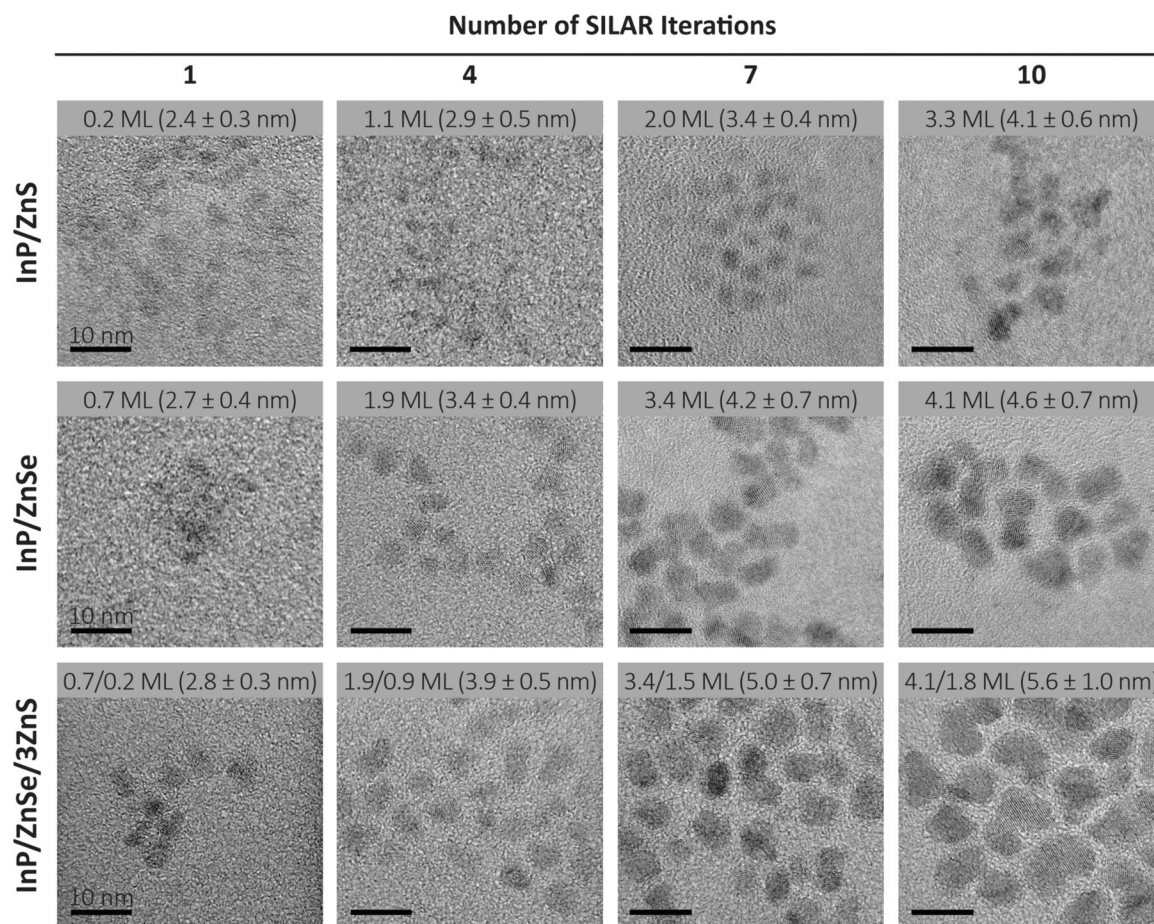
Figure 1.
Molar extinction coefficient spectra and schematic representation of (A) CdSe core nanocrystals and (B) InP core nanocrystals. Purple dashed lines denote absorbance mismatch of different QDs at the excitation wavelength (400 nm). Grey dashed lines denote the position of the 1S peak for the smallest and largest CdSe and InP core nanocrystals. Particle sizes in schematics are diameters in nm, determined using published equations to convert 1S peak position to particle size.[6]

Figure 2.
Representative TEM images of core/shell and core/shell/shell QDs after 1, 4, 7, and 10 SILAR iterations. The numbers in each image represent the number of shell monolayers deposited on each core nanocrystal, calculated based on the lattice constant of the shell material (ZnS=0.541 Å, ZnSe=0.567 Å)[6], followed by the average QD diameter and the standard deviations obtained through sizing 104–167 nanoparticles. The scale bar indicates 10 nm.
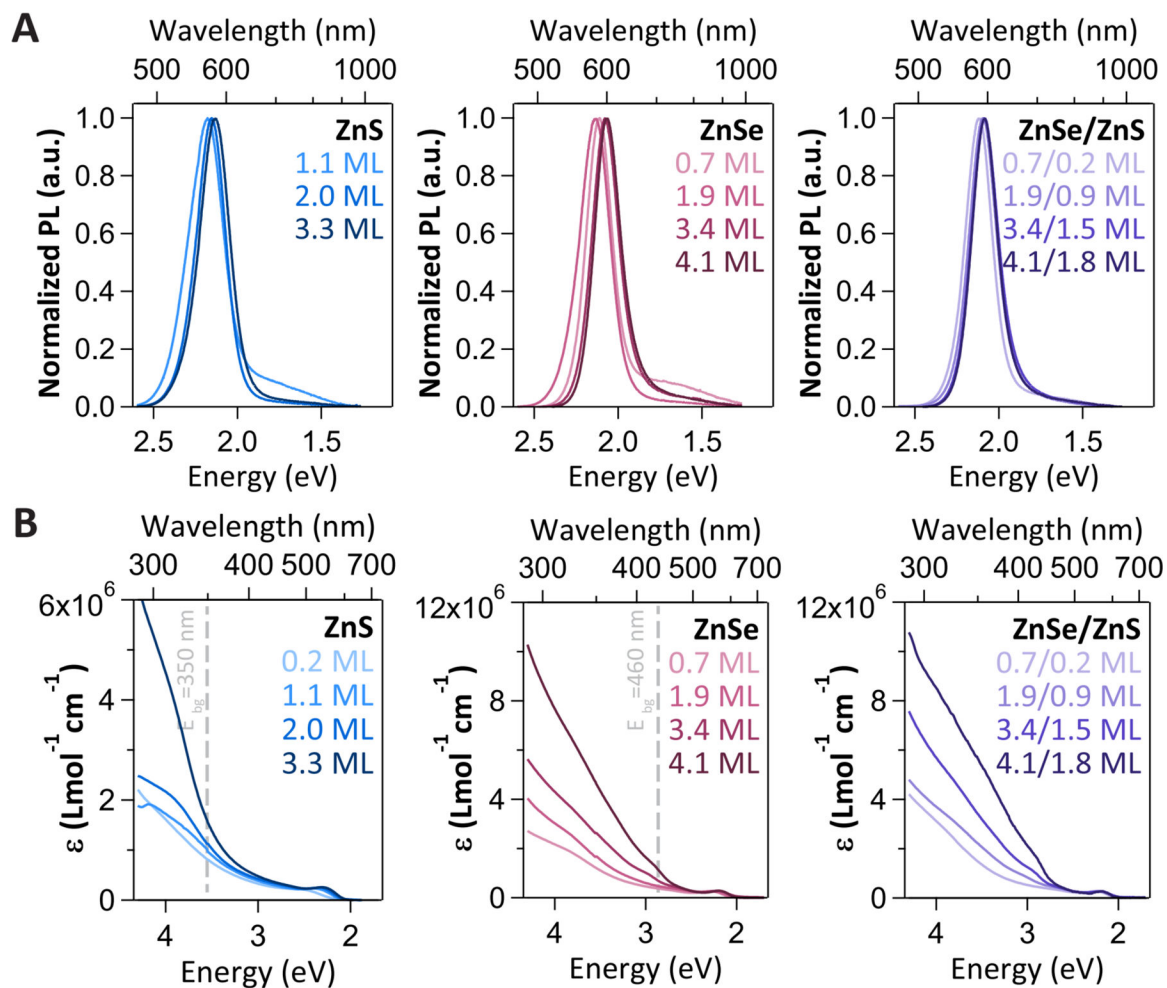
Figure 3.
(**A**) PL spectra of InP/ZnS, InP/ZnSe, and InP/ZnSe/ZnS heterostructures after 1, 4, 7, and 10 SILAR iterations following excitation at 400 nm (light to dark traces, respectively). The spectrum from the 1× SILAR InP/ZnS sample is excluded as incomplete shelling yielded only trap emission. (**B**) Molar extinction coefficients of InP/ZnS, InP/ZnSe, and InP/ZnSe/ZnS heterostructures. The dashed gray lines locate the bulk bandgap (E_{bg}) of the shell materials ($E_{bg(ZnS)} = 350$ nm; $E_{bg(ZnSe)} = 460$ nm).
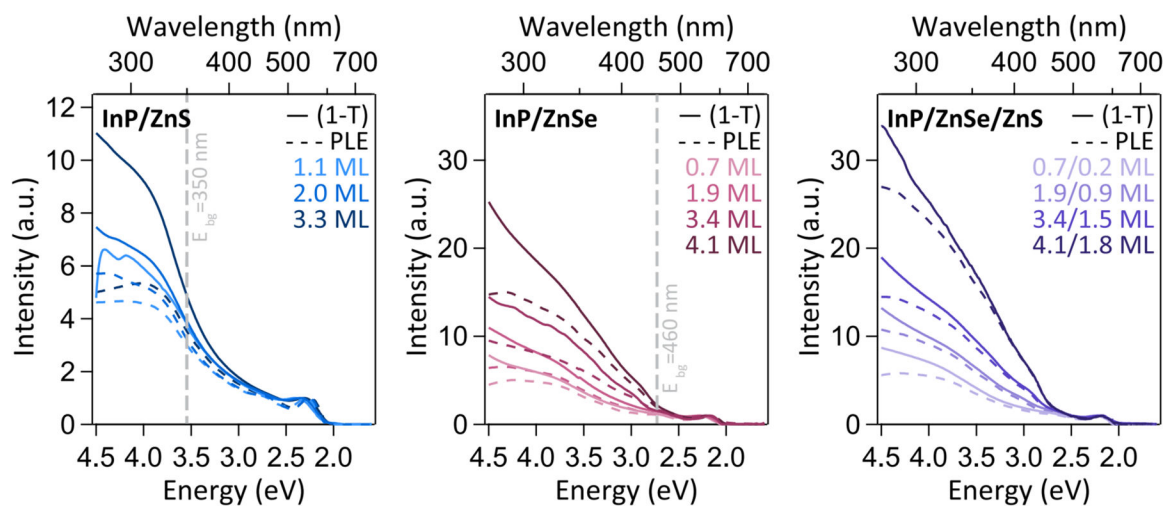
Figure 4.
Comparison of the absorption factor (1-T) spectra (solid lines) and PLE spectra (dashed lines) for InP/ZnS, InP/ZnSe, and InP/ZnSe/ZnS QDs indicates a difference between light absorbed and subsequently converted into emission across different shell compositions and thicknesses. All spectra were normalized to the 1S exciton peak.
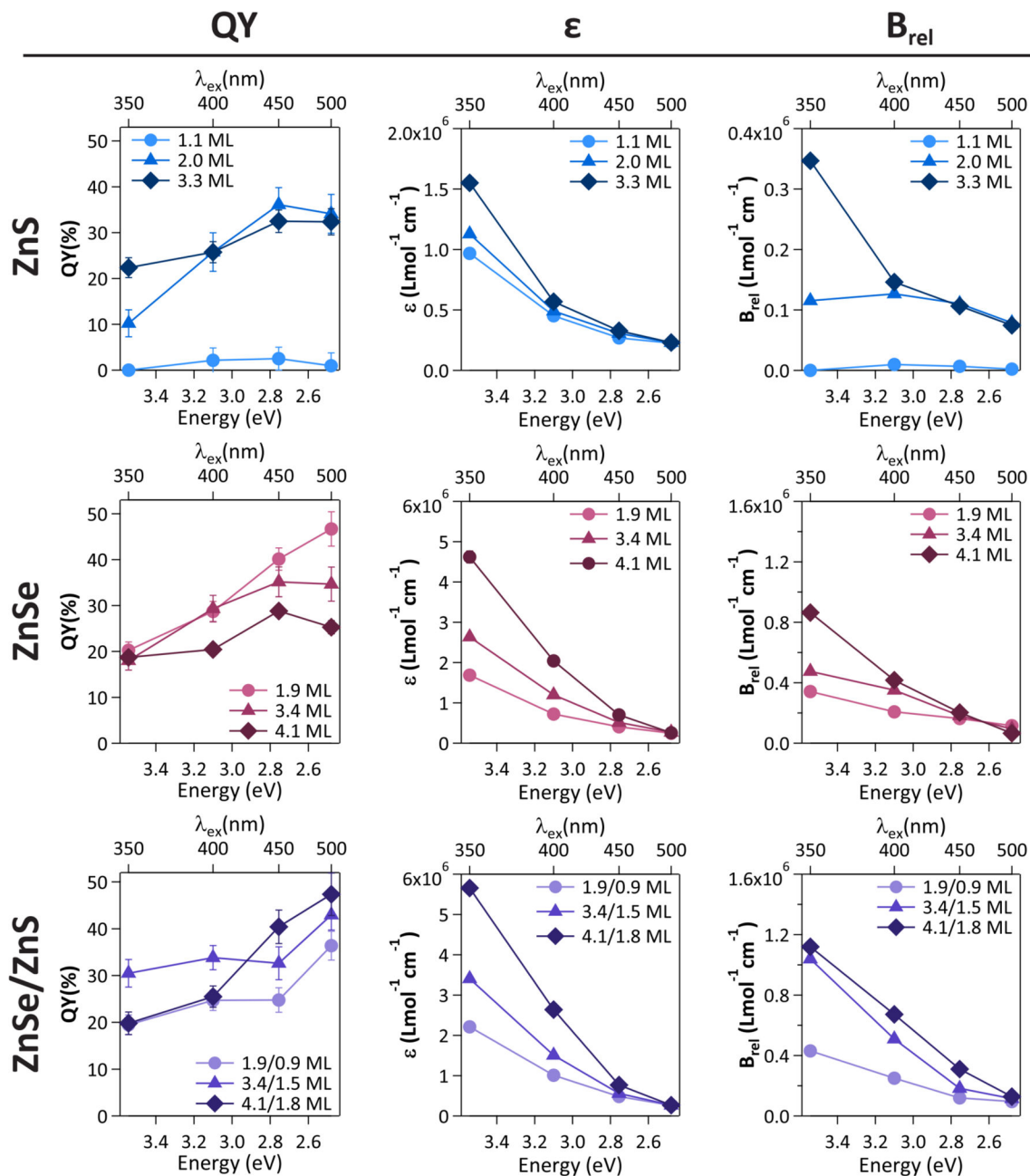
Figure 5.
QY, molar extinction coefficient (ε), and relative brightness (B_{rel}) of samples at excitation wavelengths between 350 and 500 nm.
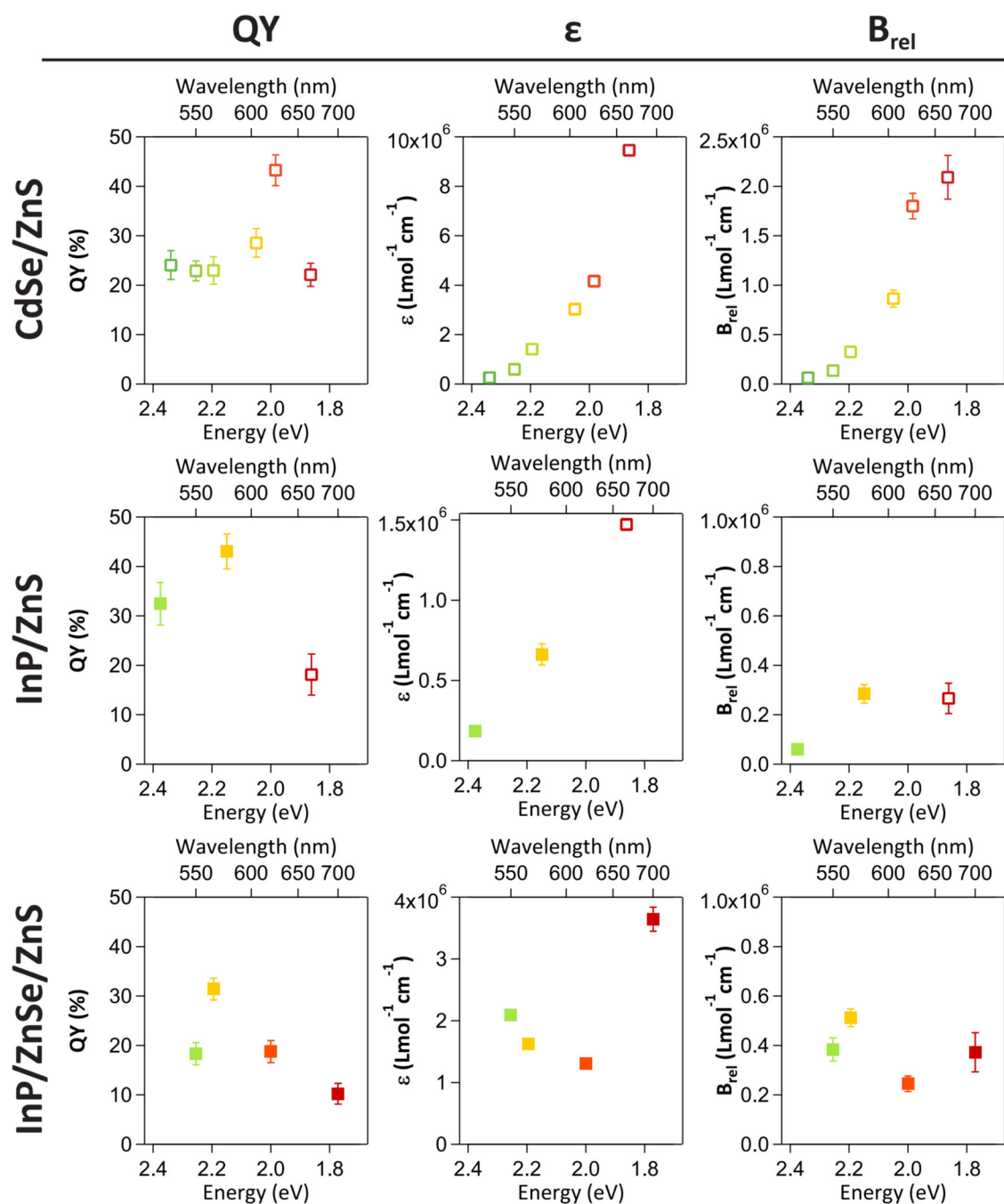
Figure 6.
QY, molar extinction coefficient, and relative brightness of CdSe/ZnS, InP/ZnS, and InP/ZnSe/ZnS emitting throughout the visible wavelength range. Open markers denote data from commercial sources and solid markers denote data from synthesized samples.[59,60]
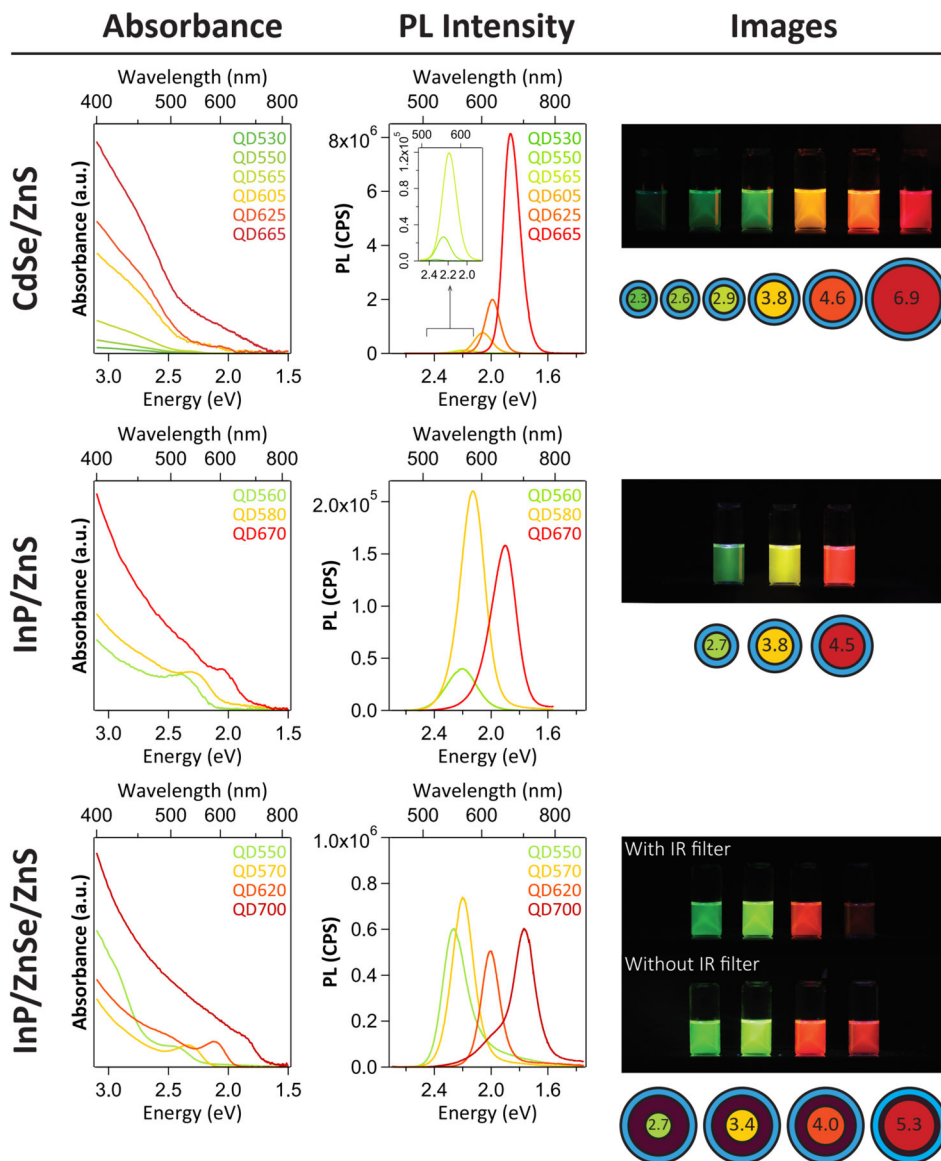
Figure 7.
Concentration-matched absorbance, concentration-matched PL spectra following excitation at 400 nm, images of samples following UV excitation (taken with and without an IR filter for InP/ZnSe/ZnS), and schematic representation of CdSe/ZnS, InP/ZnS, and InP/ZnSe/ZnS samples.

Table 1.

Summary of QD sizing information and optical properties

Sample	Diameter (nm)[a]	Shell Thickness (MLs)[b]	λ_{em} (FWHM) (nm)[c]	ε_{400} (10^6 L·mol^{-1}·cm^{-1})	fold enhancement of ε_{400} compared to InP/1ZnS[d]
InP	2.3	-	-	-	-
InP/1ZnS	2.4 ± 0.3 (14%)	0.2 ZnS	565 (-)	0.39	1.0
InP/4ZnS	2.9 ± 0.5 (17%)	1.1 ZnS	569 (64)	0.45	1.2
InP/7ZnS	3.4 ± 0.4 (11%)	2.0 ZnS	575 (54)	0.49	1.3
InP/10ZnS	4.1 ± 0.6 (14%)	3.3 ZnS	582 (57)	0.57	1.5
InP/1ZnSe	2.7 ± 0.4 (16%)	0.7 ZnSe	587 (51)	0.54	1.4
InP/1ZnSe/3ZnS	2.8 ± 0.3 (11%)	+ 0.2 ZnS	585 (52)	0.62	1.6
InP/4ZnSe	3.4 ± 0.4 (13%)	1.9 ZnSe	581 (58)	0.72	1.9
InP/4ZnSe/3ZnS	3.9 ± 0.5 (12%)	+ 0.9 ZnS	593 (55)	1.01	2.6
InP/7ZnSe	4.2 ± 0.7 (16%)	3.4 ZnSe	597 (54)	1.20	3.1
InP/7ZnSe/3ZnS	5.0 ± 0.7 (13%)	+ 1.5 ZnS	595 (55)	1.51	3.9
InP/10ZnSe	4.6 ± 0.7 (15%)	4.1 ZnSe	599 (54)	2.04	5.3
InP/10ZnSe/3ZnS	5.6 ± 1.0 (17%)	+ 1.8 ZnS	596 (51)	2.64	6.8

[a] Diameter of InP core nanocrystals was determined using an empirical fit equation.[42] Average diameter of core/shell and core/shell/shell heterostructures is determined with TEM image analysis. Average ± standard deviation (percent deviation) of 104–153 measurements.

[b] Shell thickness determined from TEM-based diameters reported in atomic MLs using ML thicknesses of 0.27 and 0.28 nm for zinc blende ZnS and ZnSe, respectively.

[c] PL peak position of samples following excitation at 400 nm.

[d] Fold enhancement of ε_{400} calculated by dividing the value of ε_{400} for each individual sample with that of InP/1ZnS.